NASA TECHNICAL MEMORANDUM

NASA TM X-1487

NASA TM X-1487

EXPERIMENTAL PRESSURE DISTRIBUTIONS AND AERODYNAMIC CHARACTERISTICS OF A LOW-FINENESS-RATIO CYLINDER AT A MACH NUMBER OF 10.5 AND ANGLES OF ATTACK FROM 0° TO 90°

by Thomas A. Blackstock and Philip E. Everhart

Langley Research Center
Langley Station, Hampton, Va.

NATIONAL AERONAUTICS AND SPACE ADMINISTRATION • WASHINGTON, D. C. • DECEMBER 1967

NASA TM X-1487

EXPERIMENTAL PRESSURE DISTRIBUTIONS AND AERODYNAMIC CHARACTERISTICS OF A LOW-FINENESS-RATIO CYLINDER AT A MACH NUMBER OF 10.5 AND ANGLES OF ATTACK FROM 0^{o} TO 90^{o}

By Thomas A. Blackstock and Philip E. Everhart

Langley Research Center
Langley Station, Hampton, Va.

NATIONAL AERONAUTICS AND SPACE ADMINISTRATION

For sale by the Clearinghouse for Federal Scientific and Technical Information
Springfield, Virginia 22151 – CFSTI price $3.00

EXPERIMENTAL PRESSURE DISTRIBUTIONS AND AERODYNAMIC CHARACTERISTICS OF A LOW-FINENESS-RATIO CYLINDER AT A MACH NUMBER OF 10.5 AND ANGLES OF ATTACK FROM 0° TO 90°

By Thomas A. Blackstock and Philip E. Everhart
Langley Research Center

SUMMARY

An investigation was made in the Langley continuous-flow hypersonic tunnel at a Mach number of 10.5 to measure the surface pressures and the force and moment characteristics of a fuel capsule designed for use on the Nimbus B weather satellite. The capsule, a fineness-ratio-2 cylinder with a recessed face, was tested at angles of attack from 0° to 90° at a Reynolds number of 0.8×10^6 based on free-stream conditions and cylinder length. At angles of attack from 37° to 90°, forces and moments were also measured on a corresponding cylinder with a flat face.

Pressures on the recessed face reached a maximum at angles of attack from 40° to 50°. Significant end effects on the pressure were concentrated within 1/2 diameter of the end of the cylinder. Analysis of the results indicated that normal force can be predicted within 15 percent by modified Newtonian theory. Agreement between experiment and theory for axial force was good near angles of attack of 0° and 90°, but the calculated results were generally somewhat low at other attitudes. The high pressure induced by the lip of the recess also produced a moderate increase in axial force, but had little effect on normal force. The recessed face greatly affected the pitching moment where large increases over the values for the flat-faced cylinder were noted.

INTRODUCTION

The fuel capsule of the Nimbus B weather satellite, a fineness-ratio-2 cylinder with a recessed face, was designed to withstand a free-fall impact during any booster abort, but to be destroyed at high altitudes by aerodynamic heating during reentry. Because of a lack of pressure and heat-transfer data for this shape, tests at varying hypersonic Mach numbers and Reynolds numbers were proposed. As part of this program, aerodynamic heat transfer to the capsule was measured at a free-stream Mach number of 10.4 (ref. 1). Force and moment data at a low Reynolds number are presented in reference 2.

The present investigation provides aerodynamic force and moment data and pressure distributions on the fuel capsule at a Mach number of 10.5 and at angles of attack from 0^{o} to 90^{o}. The investigation was conducted in the Langley continuous-flow hypersonic tunnel at a Reynolds number based on free-stream conditions and cylinder length of 0.8×10^{6}.

SYMBOLS

The units used for the physical quantities defined in this paper are given both in U.S. Customary Units and in the International System of Units (SI). Factors relating these two systems of units are presented in reference 3.

A	reference area, $\frac{\pi d^2}{4}$
C_A	axial-force coefficient, $\frac{\text{Axial force}}{q_\infty A}$
C_D	drag coefficient, $\frac{\text{Drag}}{q_\infty A}$
C_L	lift coefficient, $\frac{\text{Lift}}{q_\infty A}$
C_m	pitching-moment coefficient, $\frac{\text{Pitching moment}}{q_\infty A l}$
C_N	normal-force coefficient, $\frac{\text{Normal force}}{q_\infty A}$
C_p	pressure coefficient, $\frac{p - p_\infty}{q_\infty}$
$C_{p,max}$	maximum theoretical pressure coefficient, $\frac{\gamma + 3}{\gamma + 1}$
d	diameter of cylinder
L/D	lift-drag ratio, $\frac{C_L}{C_D}$
l	length of cylinder
p	local pressure

p_∞ free-stream static pressure

q_∞ free-stream dynamic pressure

r radius of cylinder

s distance from center of face of cylinder (see fig. 2(c))

α angle of attack measured relative to axial center line of model

γ ratio of specific heats (1.4)

ϕ radial angle about body axis (see fig. 2(c))

APPARATUS AND TESTS

Tunnel

The tests were conducted in the Langley continuous-flow hypersonic tunnel (see fig. 1(a)) at a nominal Mach number of 10.5. The test air is heated by an electrical-resistance-tube heater to avoid liquefaction when expanded through a contoured, three-dimensional, water-cooled nozzle to test conditions in a 31-inch-square (78.74-centimeter) test section. A schematic diagram of the facility is shown in figure 1(b). Starting as a blowdown tunnel using bottled air and a vacuum sphere and transferring to the compressor circuit as the area of the second minimum is reduced, the tunnel is capable of continuous operation on the closed loop.

Models

Three fuel-capsule models having a recessed face and constructed from AISI 321 stainless steel were used in this investigation. Two of the models were used for the force and stability tests at angles of attack from 0° to 90°; one was base-mounted (fig. 2(a)), whereas the other was side-mounted as shown in figure 2(b). These two models were also tested with a flat metal disk covering the recessed face.

The pressure model used over the entire 90° angle-of-attack range is shown in figure 2(c). The pressure model was instrumented with 48 orifices installed as shown in figure 2(c) and was supported by a sting attached to the base of the model.

Tests

A water-cooled internal balance was mounted on a 30° offset rotating sting as shown in figures 3(a) and 3(b). Sting rotation in conjunction with the 27° travel of the strut provides an effective angle-of-attack range of approximately 55°. Balance outputs were measured by a null-balance potentiometer with a digital output and were recorded on a card-punch and tabulator system. The maximum estimated errors for the force and moment data based on the balance inaccuracy were ± 0.04 for C_N and C_A, and ± 0.005 for C_m. Average test conditions for the program were as follows: a Mach number of 10.46, a Reynolds number of 0.76×10^6 based on free-stream conditions and cylinder length, a stagnation pressure of 80 atmospheres and a stagnation temperature of 1350° F (1006° K).

The pressure distribution studies were made by use of a mechanism which injects the model through the window opening on the right side of the nozzle. This installation, shown in figure 3(c), permits a 90° range of angle of attack with a single setup. Pressures were measured by the use of four 12-port rotary selector valves, each of which was connected to three absolute pressure transducers. The lowest range transducer was a radioactive ionization gage with a full-scale range of 0.6 psia (4 kN/m^2) and the other two transducers were of the unbonded strain-gage type with full-scale ranges of 3 psia (21 kN/m^2) and 10 psia (69 kN/m^2). The pressure coefficients were calculated using the lowest range transducer with an on-scale reading. The pressures were recorded on magnetic tape with visual display on a bar-graph-type indicator and strip-chart recorder.

DISCUSSION OF RESULTS

Shadowgraphs

Figure 4 presents shadowgraphs taken during the force tests of the base-mounted and side-mounted models of the fuel capsule with the recessed face and with the flat disk covering the face. The vertical bar in all photographs is part of the window frame.

The shock profiles for angles of attack up to about 30° (fig. 4(a)) are similar to those obtained on any flat-faced cylinder. At angles of attack from 37° to 50°, however, an additional shock wave is formed as a result of flow through the face cavity (see fig. 4(b)). Comparison of the shock profiles for the base- and side-mounted cylinders indicates that there are no significant effects of sting-mounting position. In figure 4(c), the effects of the recessed face are noticeable, however, any differences at the highest angles of attack (fig. 4(d)) are obscured by the vertical bar in the photographs. At angles of attack near 90° the shock wave is curved along the entire length of the model.

Pressure Data

The measured pressure coefficients C_p at angles of attack from 0^o to 90^o are shown in figure 5 as a function of the nondimensional distance from the center of the face of the cylinder, s/d. The juncture of the cylinder face and cylindrical side is located at s/d = 0.5. The pressure orifices on the face were misalined with those on the cylinder. In the data shown in figure 5, this offset is neglected and radial angles of 1^o, 29^o, 59^o, 89^o, 134^o, and 179^o are used. Pressures on the face of the cylinder are also presented as contour plots in figure 6. Slight asymmetry of the pressure distributions on the face at an angle of attack of 0^o suggests a small angle-of-attack error or nonstable flow associated with the recessed face. The contour plots show the shift of the peak pressure first toward the forward lip ($\phi = 0$) for angles of attack up to 25^o (figs. 5(d) and 6(d)), then toward the rearward lip ($\phi = 180^o$) for higher angles of attack ($\alpha \geq 40^o$). These high-pressure regions are caused by the compression of the air in the vicinity of the steps on the cylinder face. The highest pressures on the face occurred at angles of attack between 40^o and 50^o (figs. 5(e), 5(f), 6(e), and 6(f)) and correspond to the high heat transfer at these angles of attack shown in reference 1. Peak pressures $(C_p \geq 2.2)$ considerably in excess of the pressure coefficient behind a normal shock $(C_p \approx 1.83)$ obviously result from the greater efficiency of the double-shock system resulting from flow through the recessed-face cavity. The presence of the cavity influences the face pressures at all angles of attack up to 90^o.

The pressure along the cylindrical walls increases with angle of attack for radial angles from about 0^o to 90^o and shows very little change in pressure for radial angles of approximately 135^o and 180^o for most angles of attack (fig. 5); this result is in agreement with that indicated by other swept-cylinder data. Expansion of the flow around the lip resulted in lower pressures near the forward end of the cylinder at angles of attack up to 25^o. For angles of attack from 25^o to 65^o, higher pressures were measured near the upstream end of the cylinder along windward rays; however, there is no evidence of the higher face pressure bleeding over to the leeward rays. At angles of attack greater than 65^o, the lower pressures toward the end of the windward ray reflect the expansion of the flow over the ends of the cylinder. The pressures along this ray ($\phi = 1^o$) at an angle of attack of 90^o reached the theoretical value $(C_p = 1.83)$ within 1/2 diameter of the ends of the cylinder.

Force and Moment Data

Aerodynamic data about both the body- and the stability-axis systems are presented in figure 7 and compared with modified Newtonian theory. The effect of sting position is illustrated, and data obtained on a flat-faced cylinder are also presented.

The theory presented is that referred to in reference 4 as the blunt nose modified Newtonian theory in which $C_{p,max} = \frac{\gamma + 3}{\gamma + 1}$. In the calculations it was assumed that the cylinder was flat-faced. Normal force was generally well predicted (within 15 percent). The agreement between experiment and theory for axial force was good near angles of attack of 0^o and 90^o, but the calculated values were somewhat lower than the experimental values at other angles of attack. As would be expected, the data obtained from the flat-faced cylinder were in better agreement with theory than the data from the recessed-face cylinder.

The differences between results obtained with the base-mounted cylinder and those obtained with the side-mounted cylinder are attributed to the sting interference; however, thermal distortion may cause some of the data scatter since cylinder temperatures of 1000^o F (811^o K) to 1200^o F (922^o K) were noted.

The recessed face has a strong effect on the pitching moment. The explanation for its effect can be seen in figure 8 in which the pitching moment is shown with shadowgraphs and pressure distributions along the vertical center line of the recessed face and along the length of the cylinder. At low angles of attack the pressure gradient across the face is small and the shock shape is similar to that for a flat-faced cylinder. At an angle of attack of 50^o the pitching moment and the pressure gradients across the face and down the length of the cylinder reach a maximum and the shadowgraph indicates a large amount of airflow into the cavity. As the angle of attack was increased, the pitching moment and the pressure gradients decreased. The recessed face also produced a moderate increase in axial force, but had little effect on normal force.

CONCLUDING REMARKS

An investigation was made in the Langley continuous-flow hypersonic tunnel at a Mach number of 10.5 to measure the pressure distributions and force and moment characteristics of a fuel capsule designed for use on the Nimbus B weather satellite. The capsule, a fineness-ratio-2 cylinder with a recessed face, was tested at angles of attack from 0^o to 90^o at a Reynolds number of 0.8×10^6 based on free-stream conditions and cylinder length. Forces and moments were also measured at angles of attack from 37^o to 90^o with a corresponding cylinder with a flat face.

Pressures on the recessed face reached a maximum at angles of attack from 40^o to 50^o. The significant end effects on the pressure were concentrated within 1/2 diameter of the ends of the cylinder. Analysis of the results indicates that normal force can be predicted within 15 percent by modified Newtonian theory. Agreement between experiment and theory for axial force was good near angles of attack of 0^o and 90^o, but the calculated results were generally low at other attitudes. The high pressure induced

by the lip of the recess also produced a moderate increase in axial force, but had little effect on normal force. The recessed face greatly affected the pitching moment where large increases over the values for the flat-face cylinder were noted.

Langley Research Center,
National Aeronautics and Space Administration,
Langley Station, Hampton, Va., July 14, 1967,
124-07-01-39-23.

REFERENCES

1. Everhart, Philip E.: Heat-Transfer Measurements on a Low-Fineness-Ratio Cylinder at a Mach Number of 10.4 and Angles of Attack From 0^{o} to 90^{o}. NASA TM X-1400, 1967.

2. Stouffer, C. G.: SNAP 19 Capsule Low Reynolds Number Force Test. MND-3607-89 (Contract AT(30-1)-3607), Martin Co., Oct. 1966.

3. Mechtly, E. A.: The International System of Units – Physical Constants and Conversion Factors. NASA SP-7012, 1964.

4. Love, Eugene S.; Henderson, Arthur, Jr.; and Bertram, Mitchel H.: Some Aspects of Air-Helium Simulation and Hypersonic Approximations. NASA TN D-49, 1959.

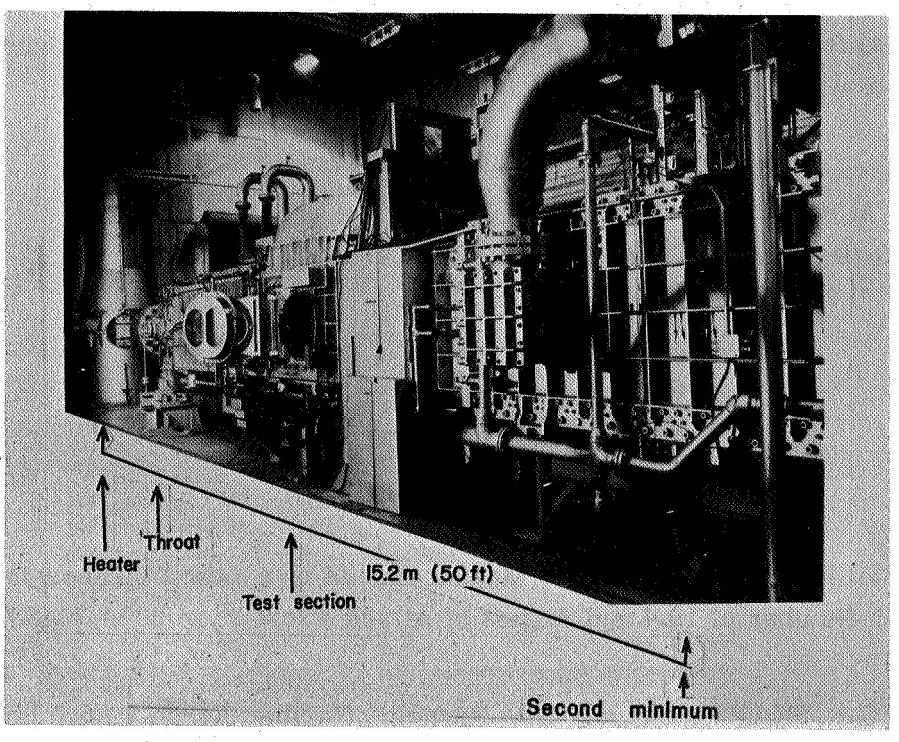

(a) General view.

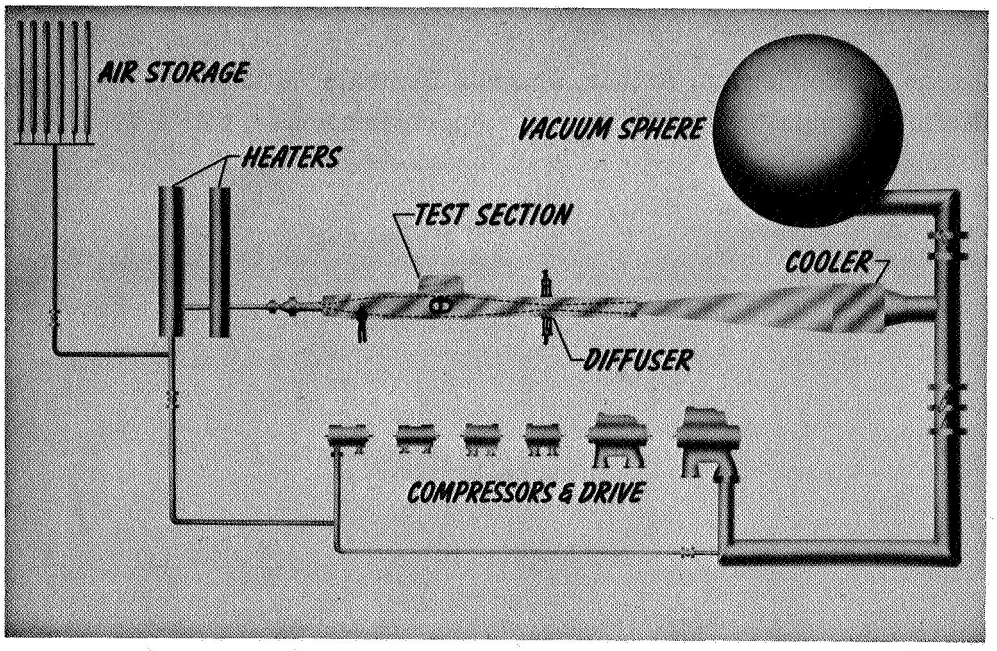

(b) Schematic diagram of the facility.

L-65-5822

Figure 1.- Langley continuous-flow hypersonic tunnel.

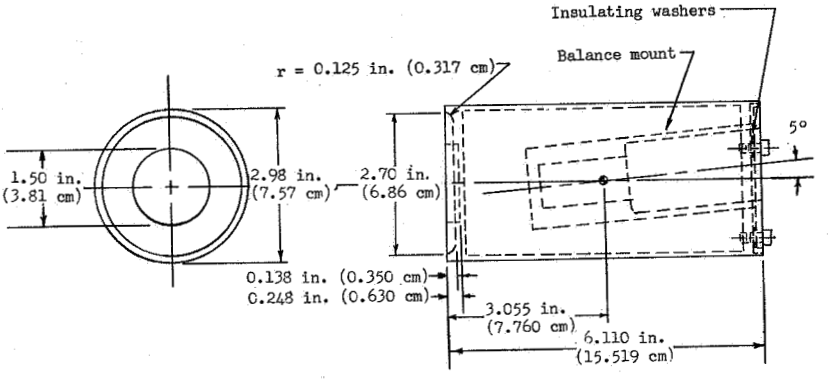

(a) Base-mounted model.

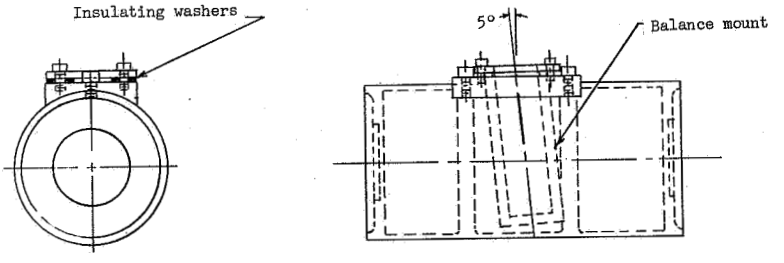

(b) Side-mounted model.

Figure 2.- Models used in investigation.

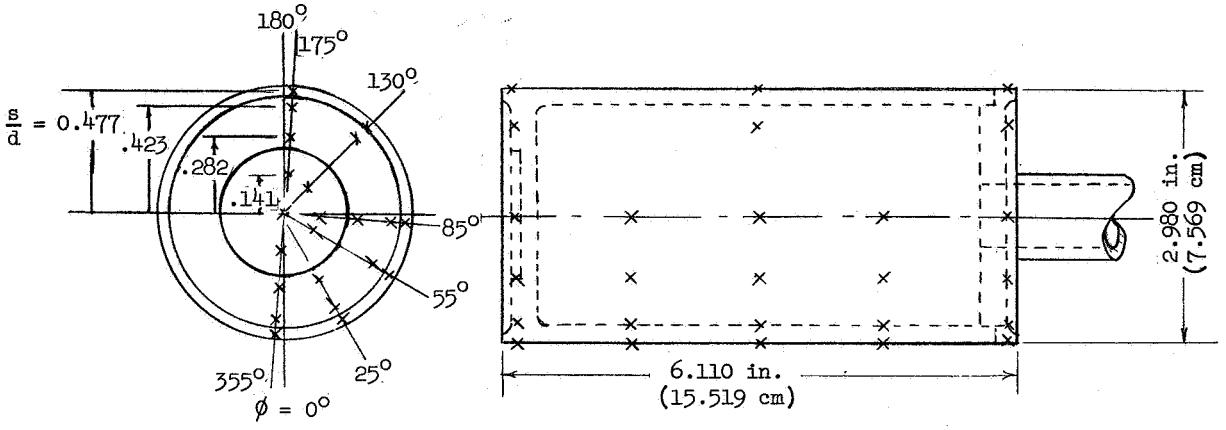

Face	
ø, deg	s/d
0	0
55	.141
85	↓
130	
175	
355	
25	0.282
85	↓
175	
355	
25	0.423
55	↓
85	
130	
175	
355	
25	0.477
55	↓
85	
130	
175	
355	
0	0.532
30	↓
60	
90	
135	
180	

Cylinder	
ø, deg	s/d
1	1.0289
29	↓
59	
89	
1	1.5255
29	↓
59	
89	
134	
179	
1	2.0221
29	↓
59	
89	
1	2.5188
29	↓
59	
89	
134	
179	

(c) Pressure model dimensions and orifice locations.

Figure 2.- Concluded.

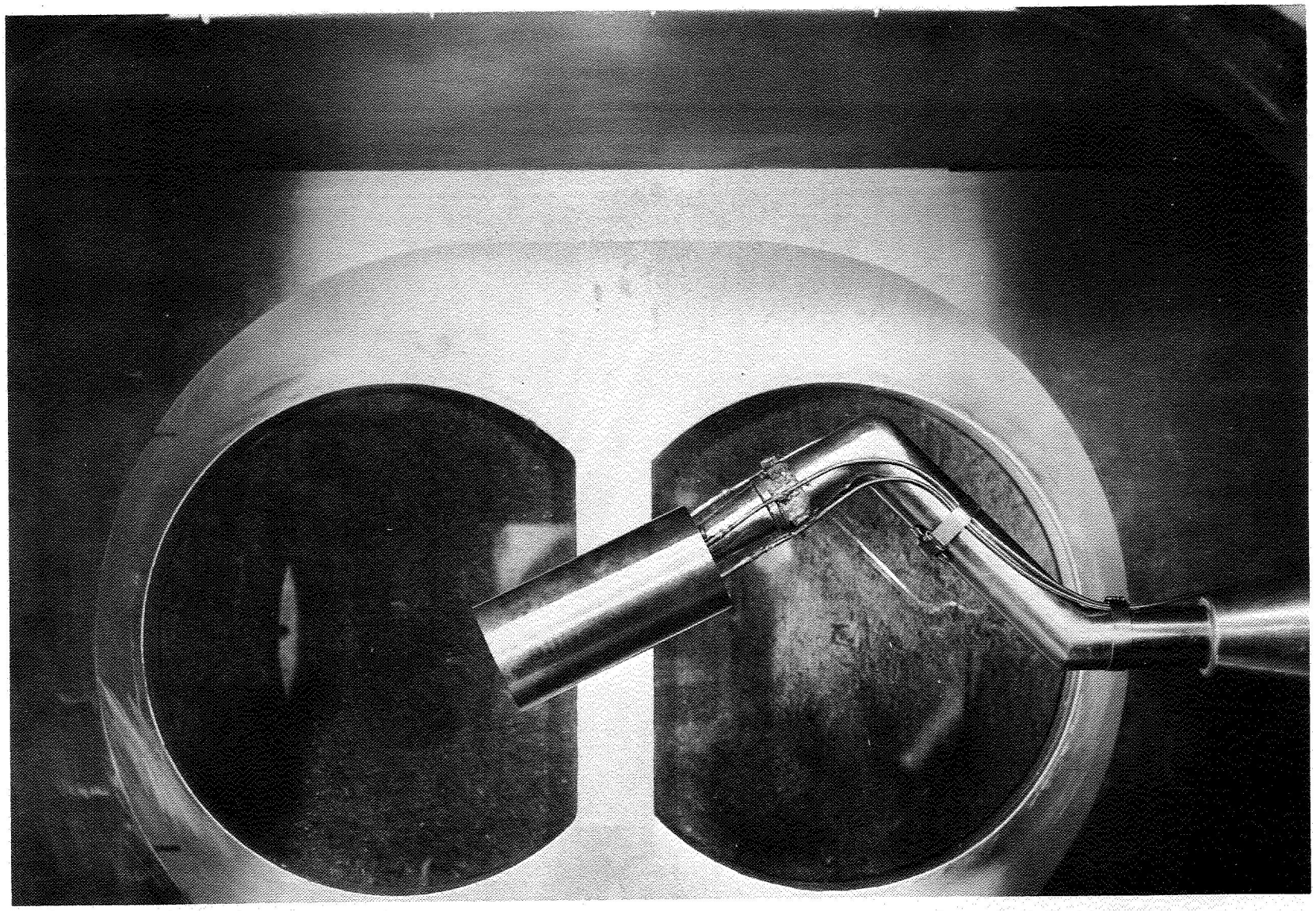

(a) Base-mounted model.

L-66-5052

Figure 3.- Model installation.

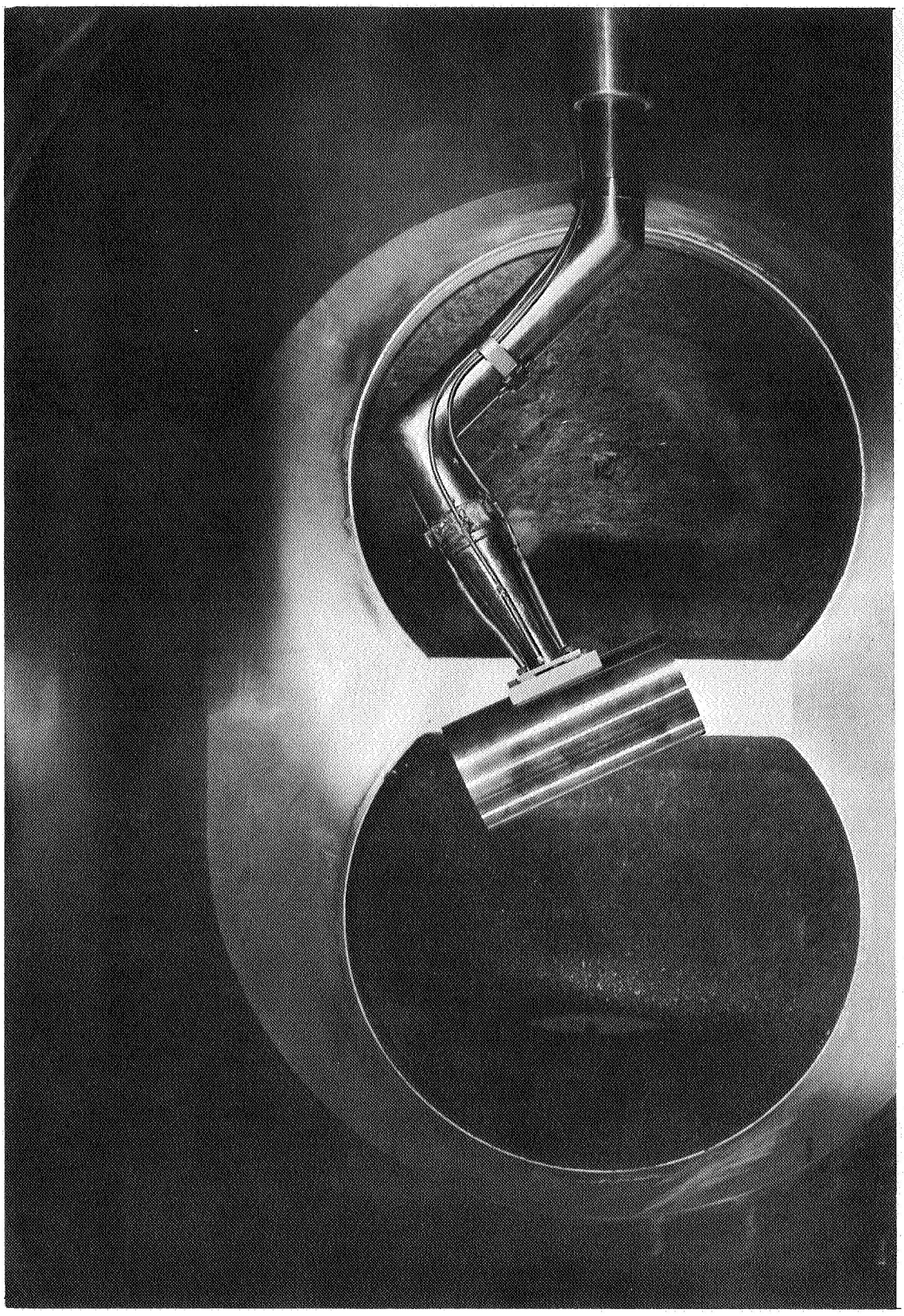

L-66-5053

(l) Side-mounted model.

Figure 3.- Continued.

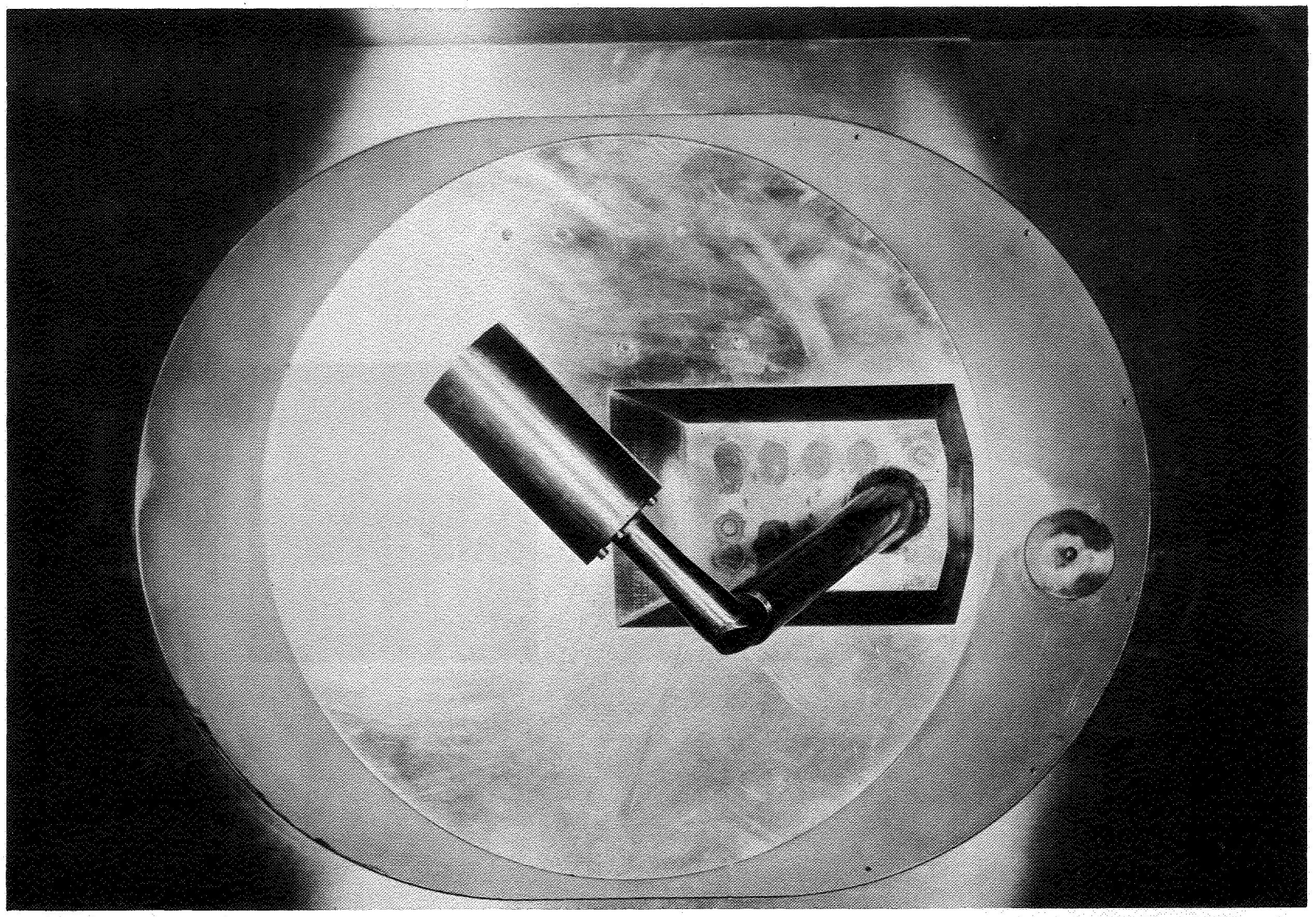

(c) Pressure model. L-66-5634

Figure 3.- Concluded.

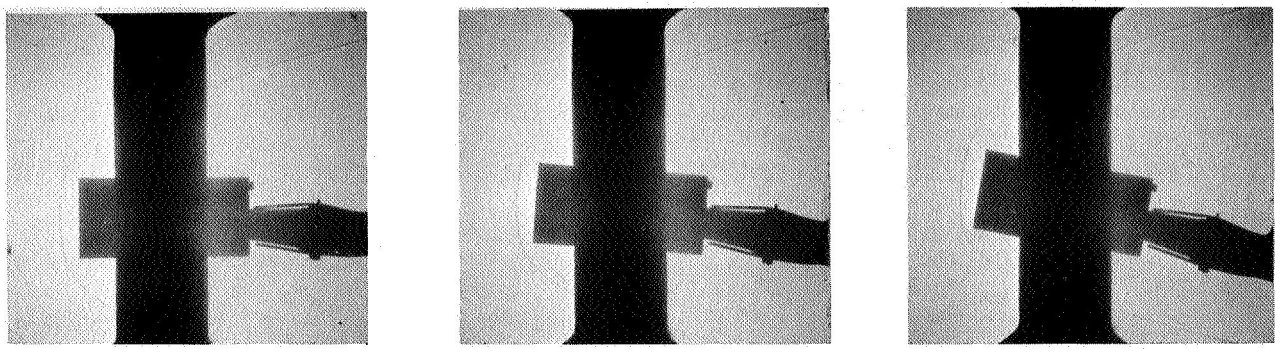

$\alpha = 1.0^{o}$ $\alpha = 6.0^{o}$ $\alpha = 11.0^{o}$

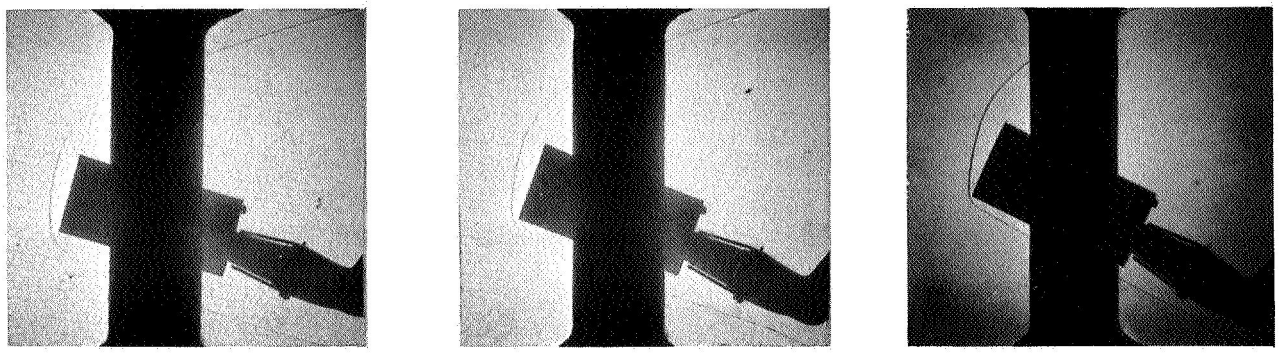

$\alpha = 16.0^{o}$ $\alpha = 21.0^{o}$ $\alpha = 25.0^{o}$

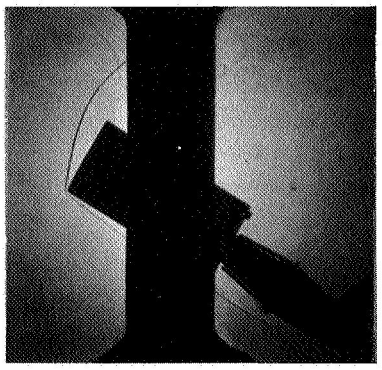

$\alpha = 30.0^{o}$

Base-mounted model

(a) $\alpha \approx 1^{o}$ to 30^{o}. L-67-6661

Figure 4.- Shadowgraphs of model of the Nimbus B fuel capsule.

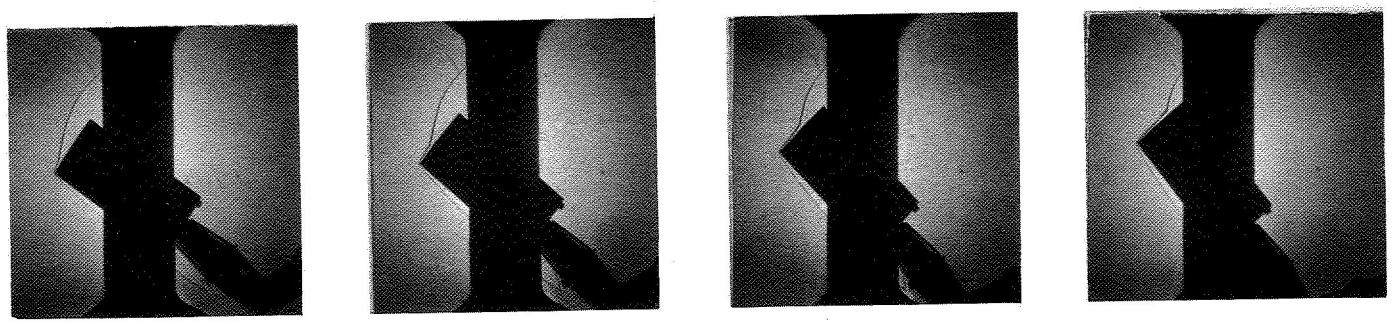

$\alpha = 35.1^{o}$ $\alpha = 40.0^{o}$ $\alpha = 45.1^{o}$ $\alpha = 50.2^{o}$

Base-mounted model

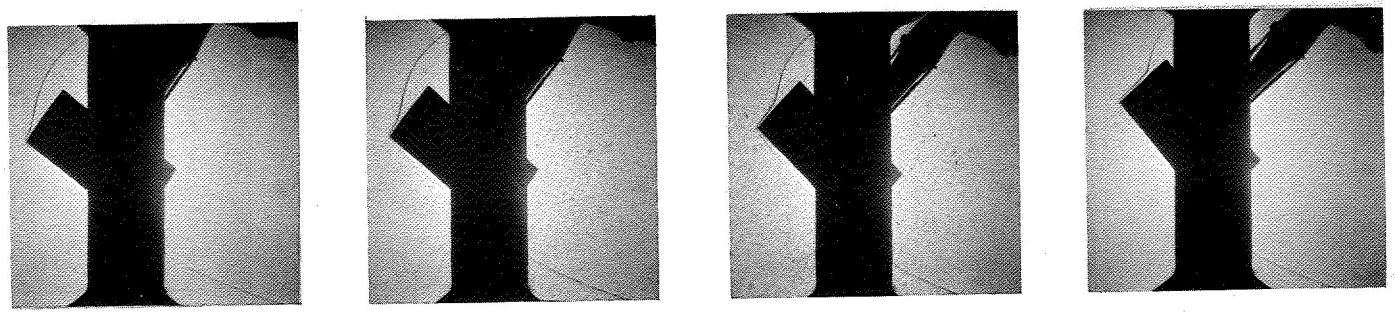

$\alpha = 37.0^{o}$ $\alpha = 40.0^{o}$ $\alpha = 45.0^{o}$ $\alpha = 50.1^{o}$

Side-mounted model

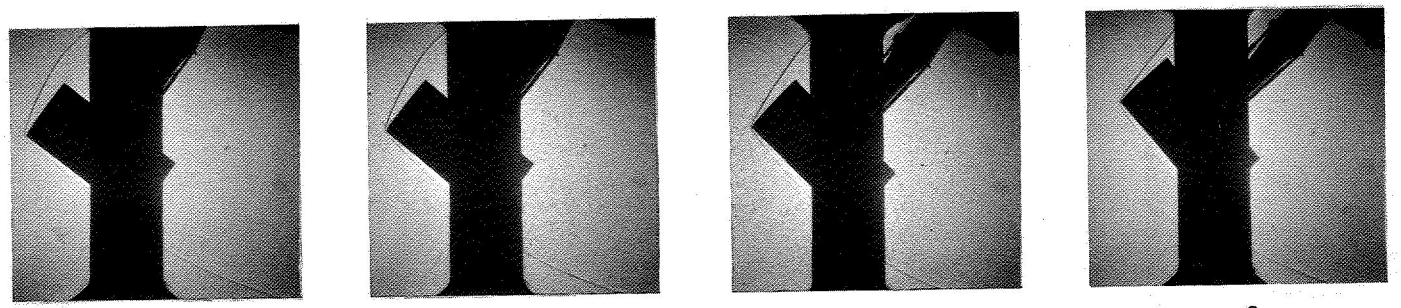

$\alpha = 37.0^{o}$ $\alpha = 39.9^{o}$ $\alpha = 45.0^{o}$ $\alpha = 50.0^{o}$

Side-mounted model with flat face

(b) $\alpha \approx 35^{o}$ to 50^{o}.

L-67-6662

Figure 4.- Continued.

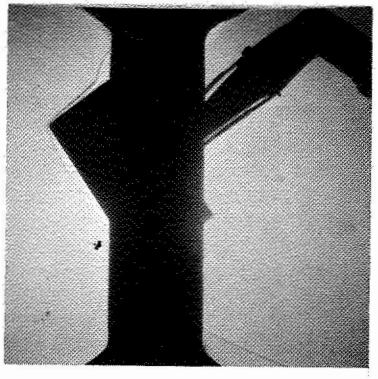

$\alpha = 55.1^{o}$

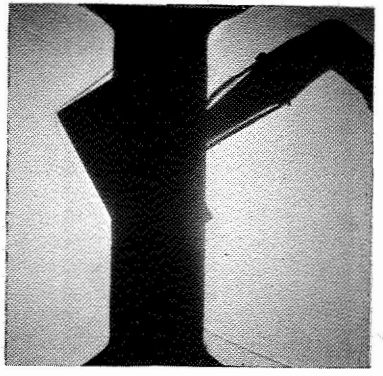

$\alpha = 60.1^{o}$

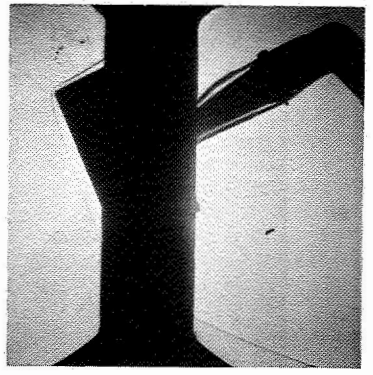

$\alpha = 65.1^{o}$

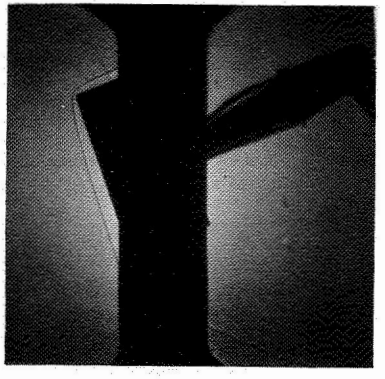

$\alpha = 70.9^{o}$

Side-mounted model

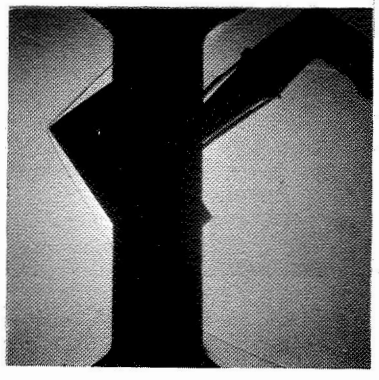

$\alpha = 55.0^{o}$

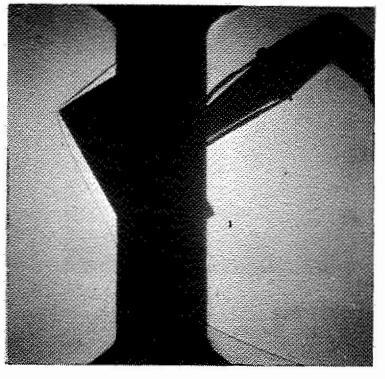

$\alpha = 60.1^{o}$

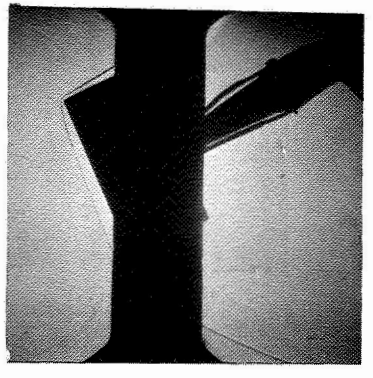

$\alpha = 65.1^{o}$

Side-mounted model with flat face

(c) $\alpha \approx 55^{o}$ to 70^{o}.

L-67-6663

Figure 4.- Continued.

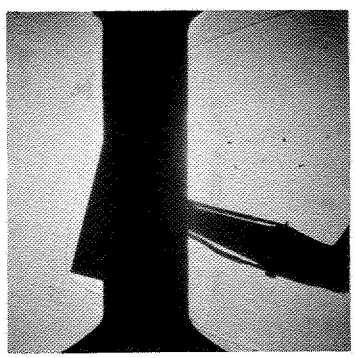

$\alpha = 75.8^{o}$

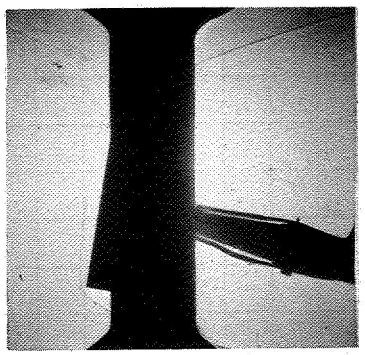

$\alpha = 80.7^{o}$

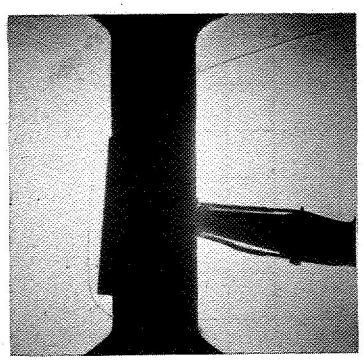

$\alpha = 85.5^{o}$

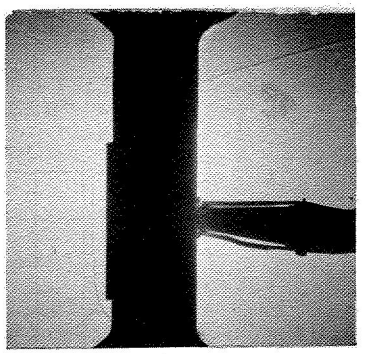

$\alpha = 90.5^{o}$

Side-mounted model

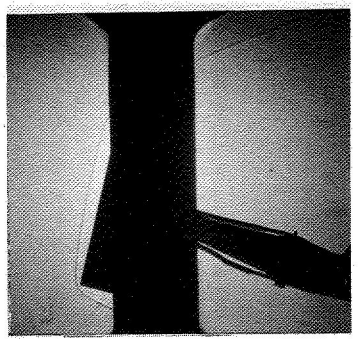

$\alpha = 74.2^{o}$

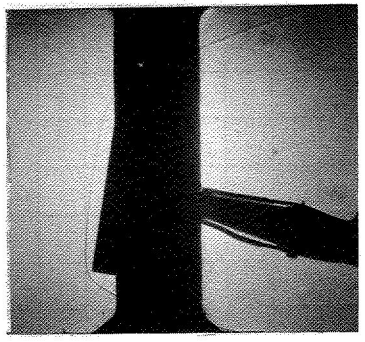

$\alpha = 79.3^{o}$

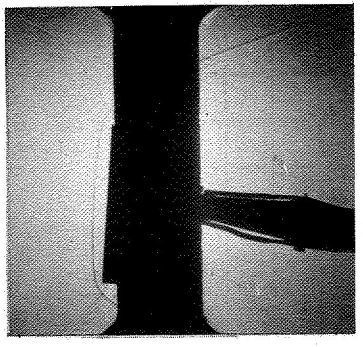

$\alpha = 84.3^{o}$

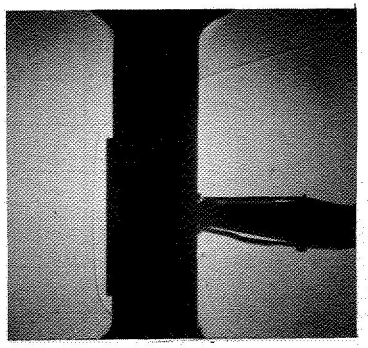

$\alpha = 89.2^{o}$

Side-mounted model with flat face

(d) $\alpha \approx 75^{o}$ to 90^{o}.

L-67-6664

Figure 4.- Concluded.

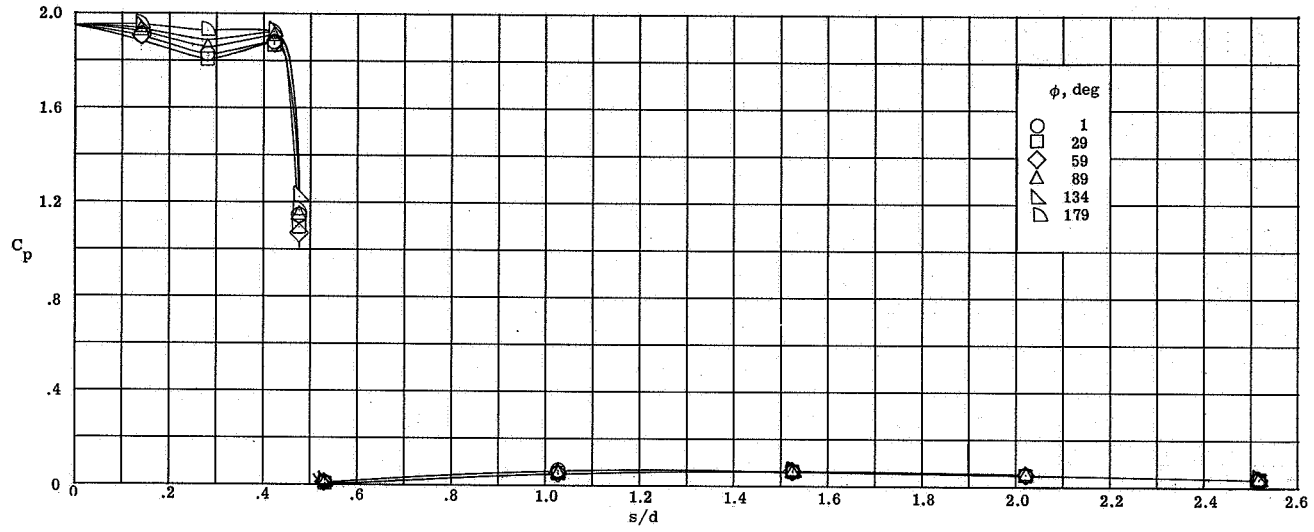

(a) $\alpha = 0^0$.

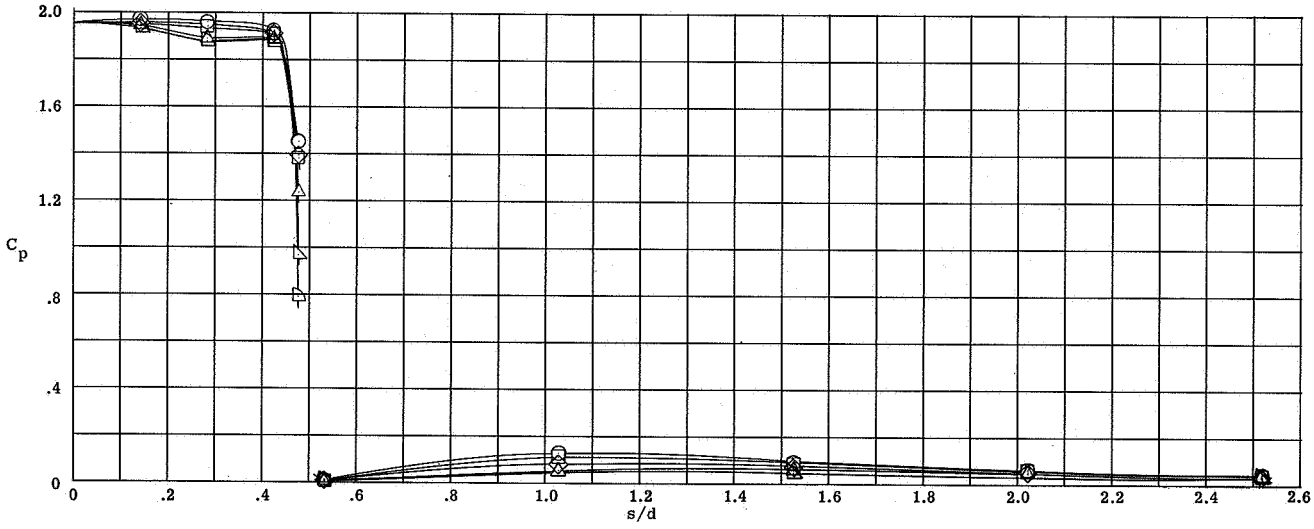

(b) $\alpha = 7.5^0$.

Figure 5.- Measured pressure coefficients on model of the Nimbus B fuel capsule with recessed face.

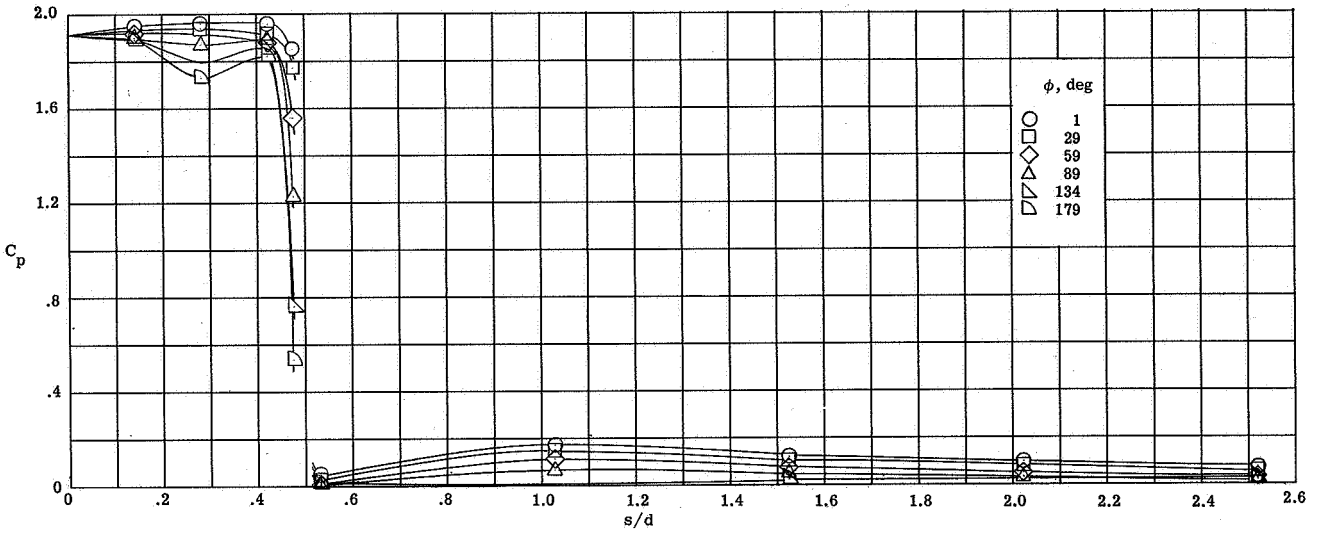

(c) $\alpha = 15.0^0$.

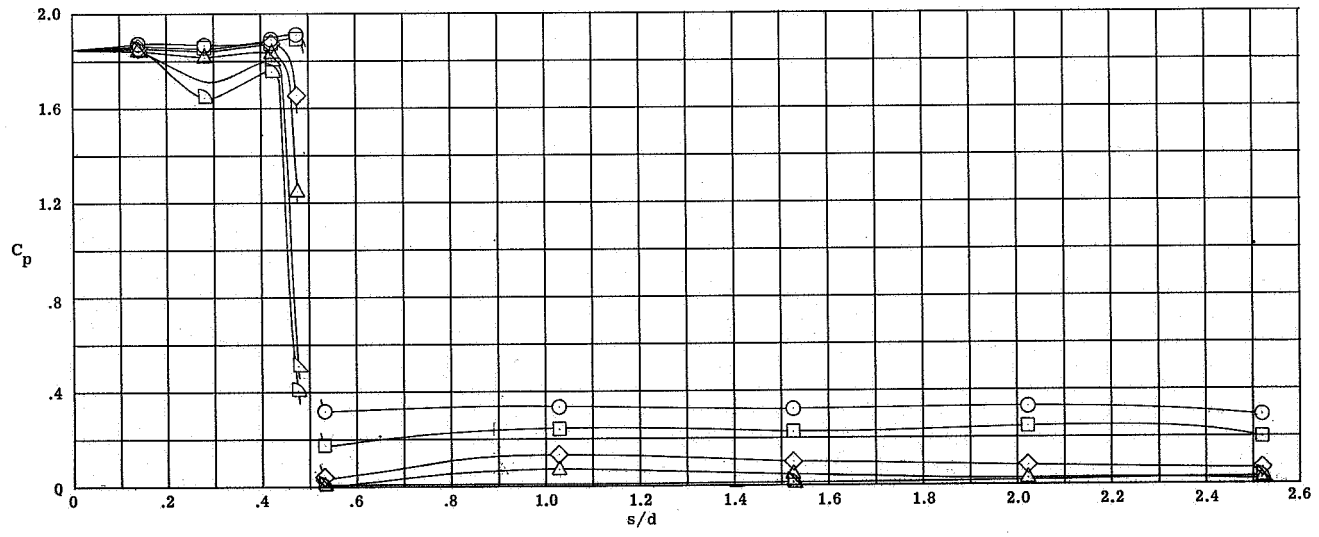

(d) $\alpha = 25.0^0$.

Figure 5.- Continued.

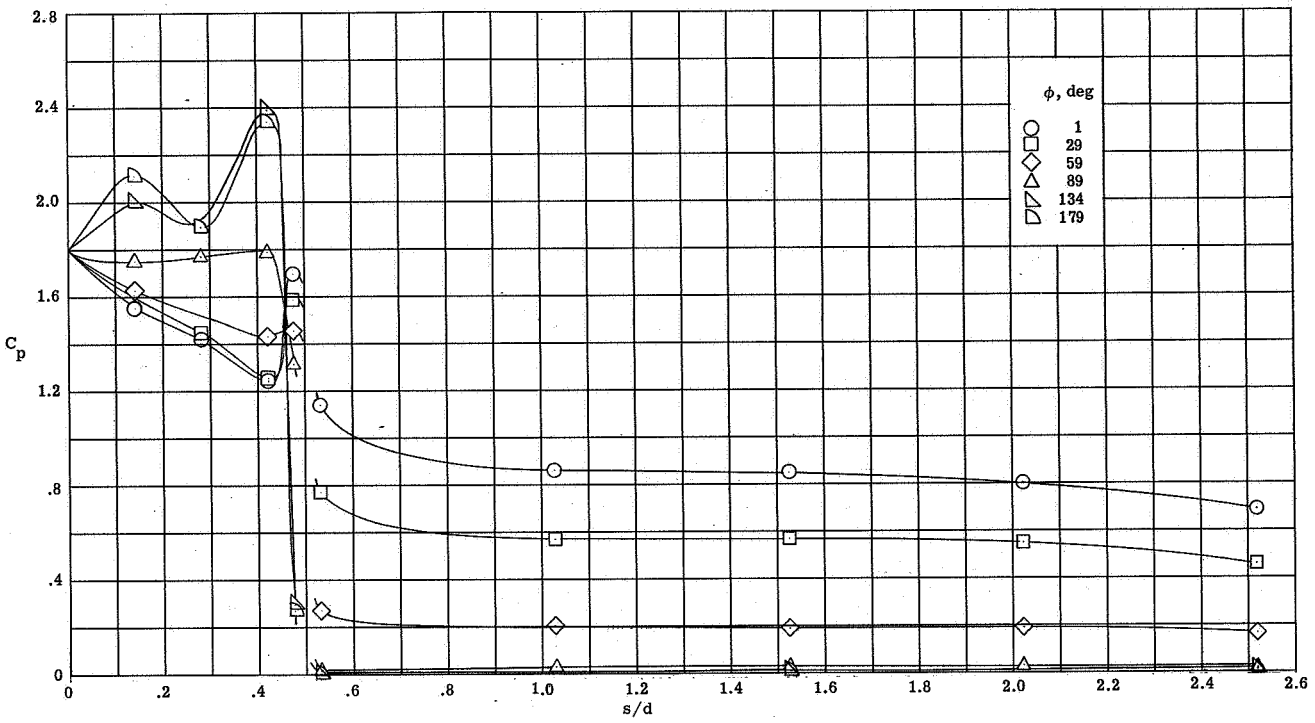

(e) $\alpha = 40.0^0$.

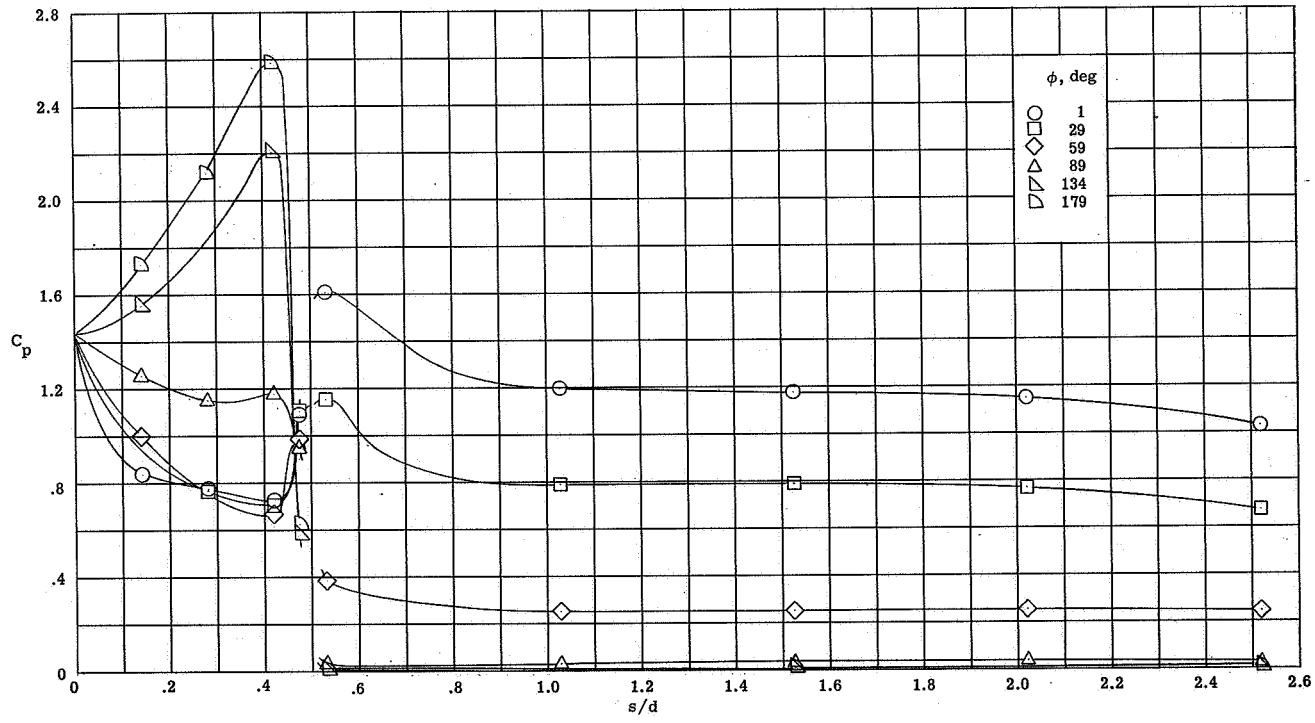

(f) $\alpha = 50.0^0$.

Figure 5.- Continued.

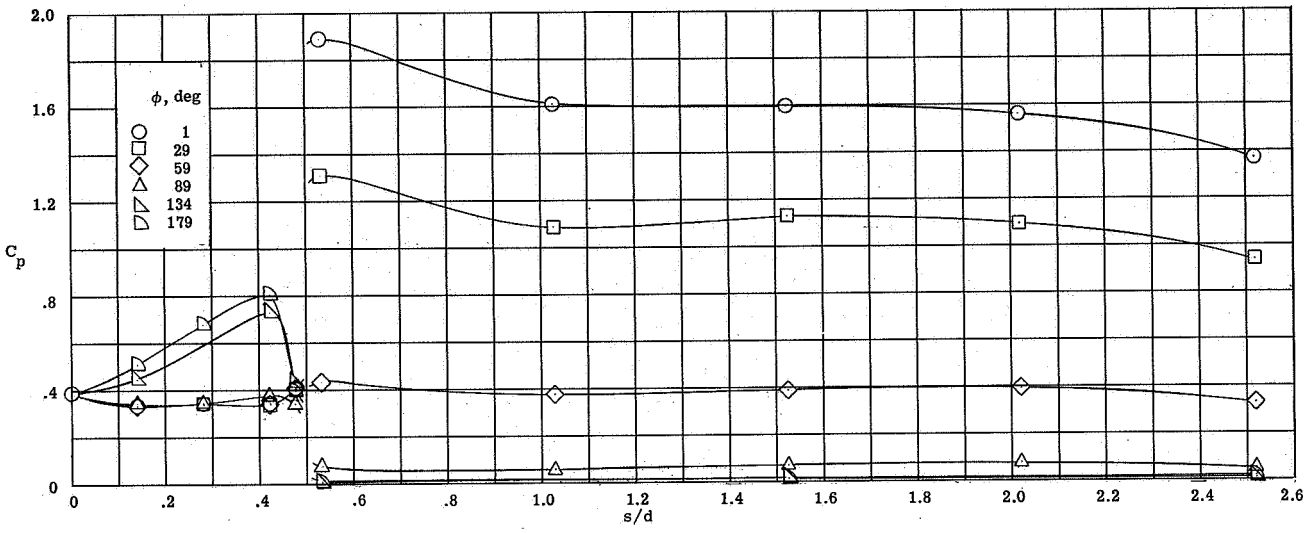

(g) $\alpha = 65.0^0$.

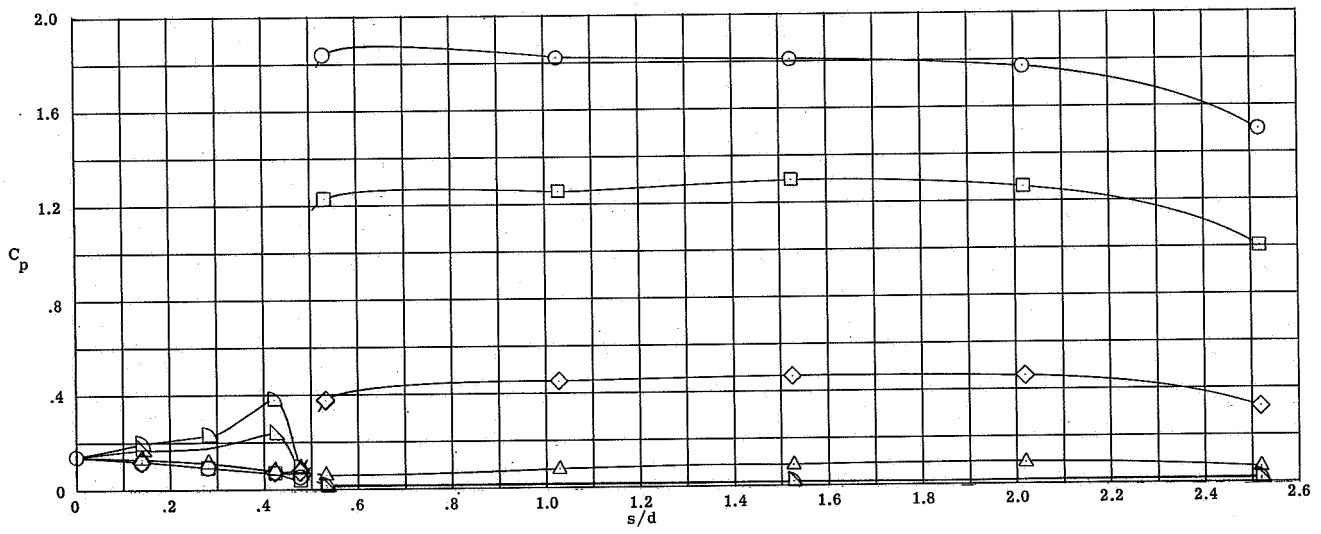

(h) $\alpha = 80.0^0$.

Figure 5.- Continued.

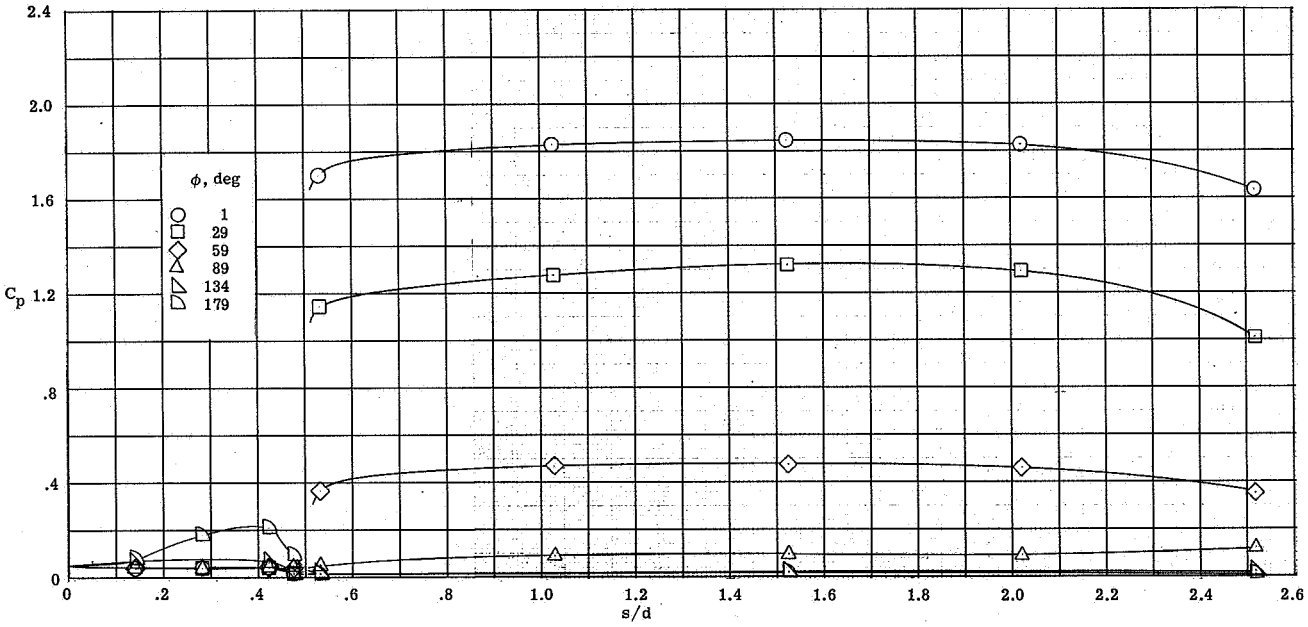

(i) $\alpha = 90.0^0$.

Figure 5.- Concluded.

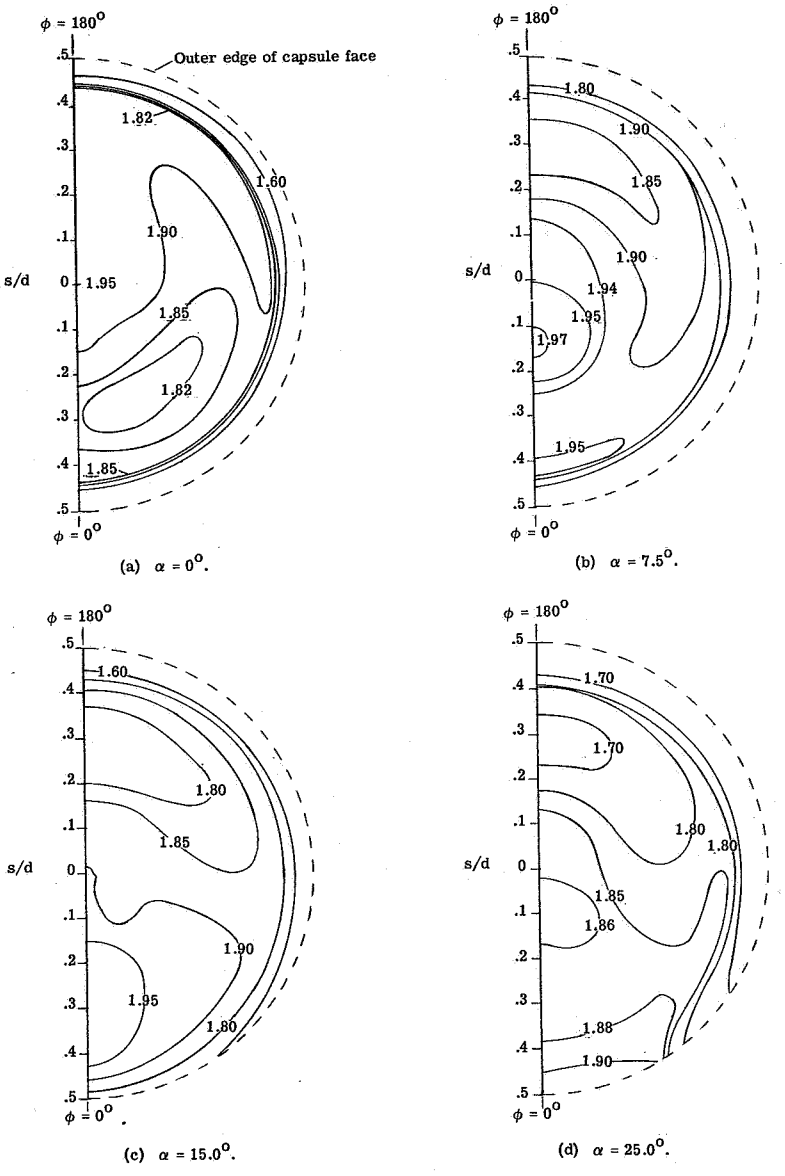

Figure 6.- Contour plots of pressure coefficients on the recessed face of the cylinder.

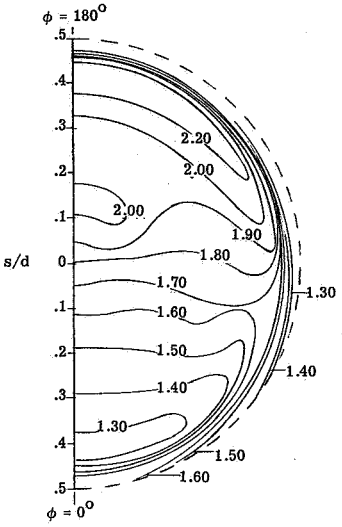

(e) $\alpha = 40.0^o$.

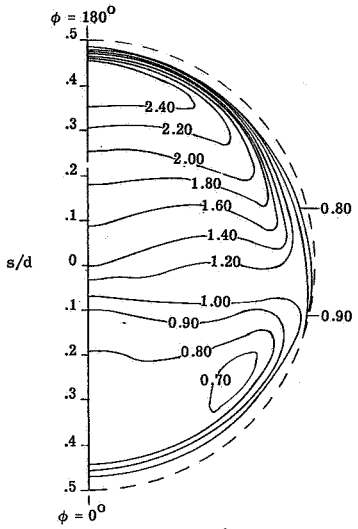

(f) $\alpha = 50.0^o$.

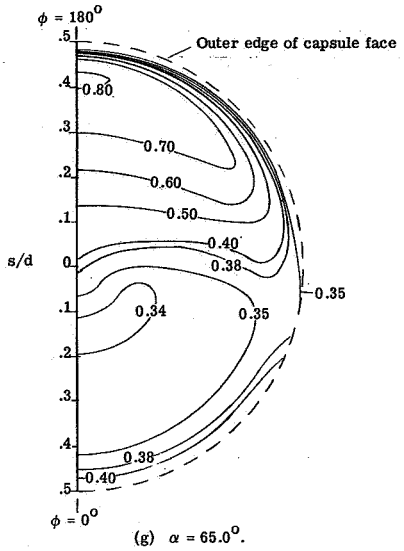

(g) $\alpha = 65.0^o$.

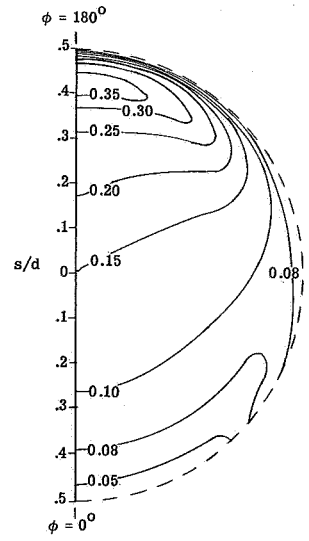

(h) $\alpha = 80.0^o$.

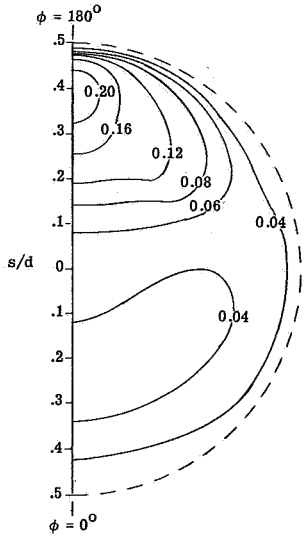

(i) $\alpha = 90.0^o$.

Figure 6.- Concluded.

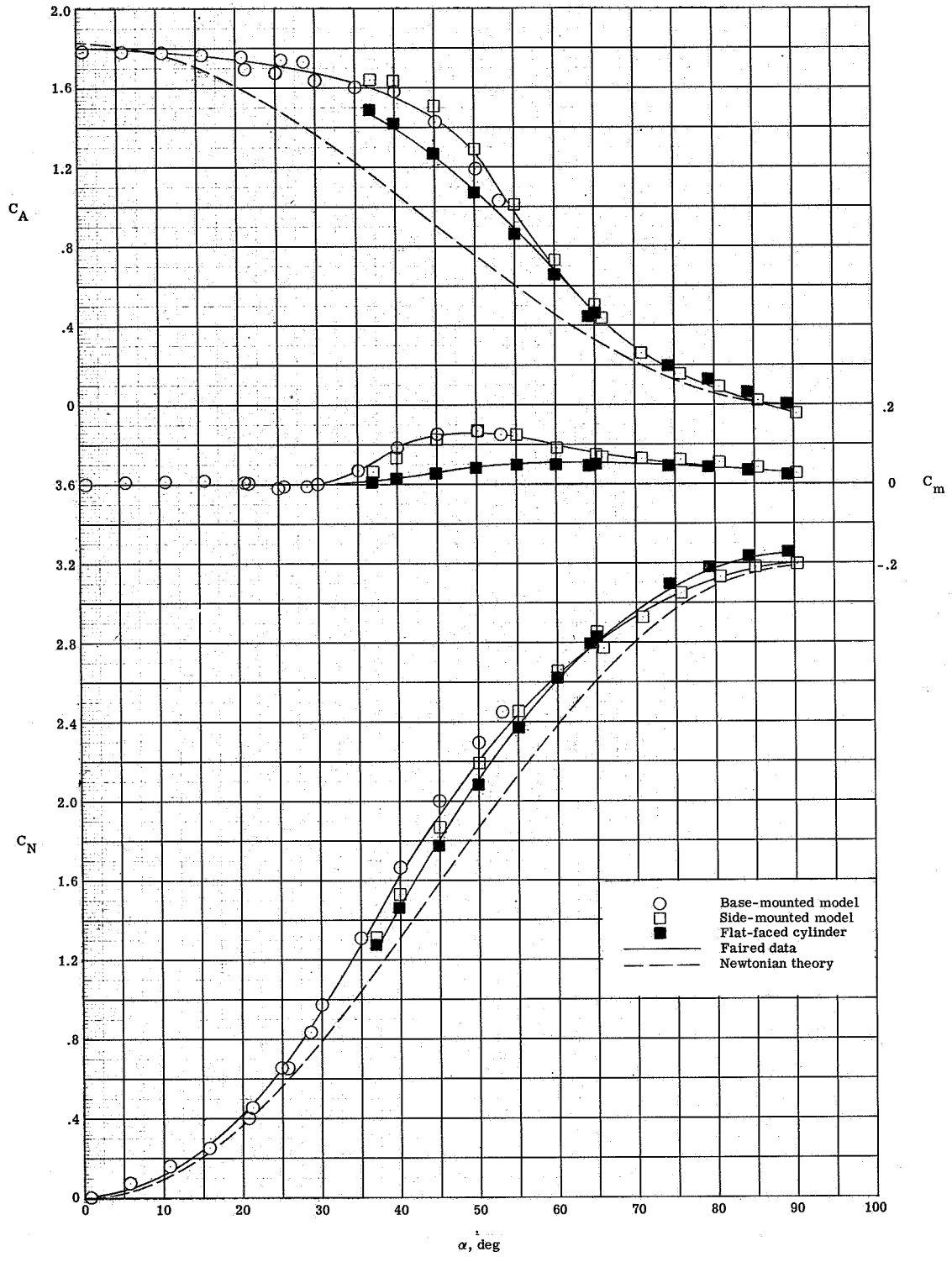

(a) Body-axis data.

Figure 7.- Aerodynamic characteristics of model of the Nimbus B fuel capsule.

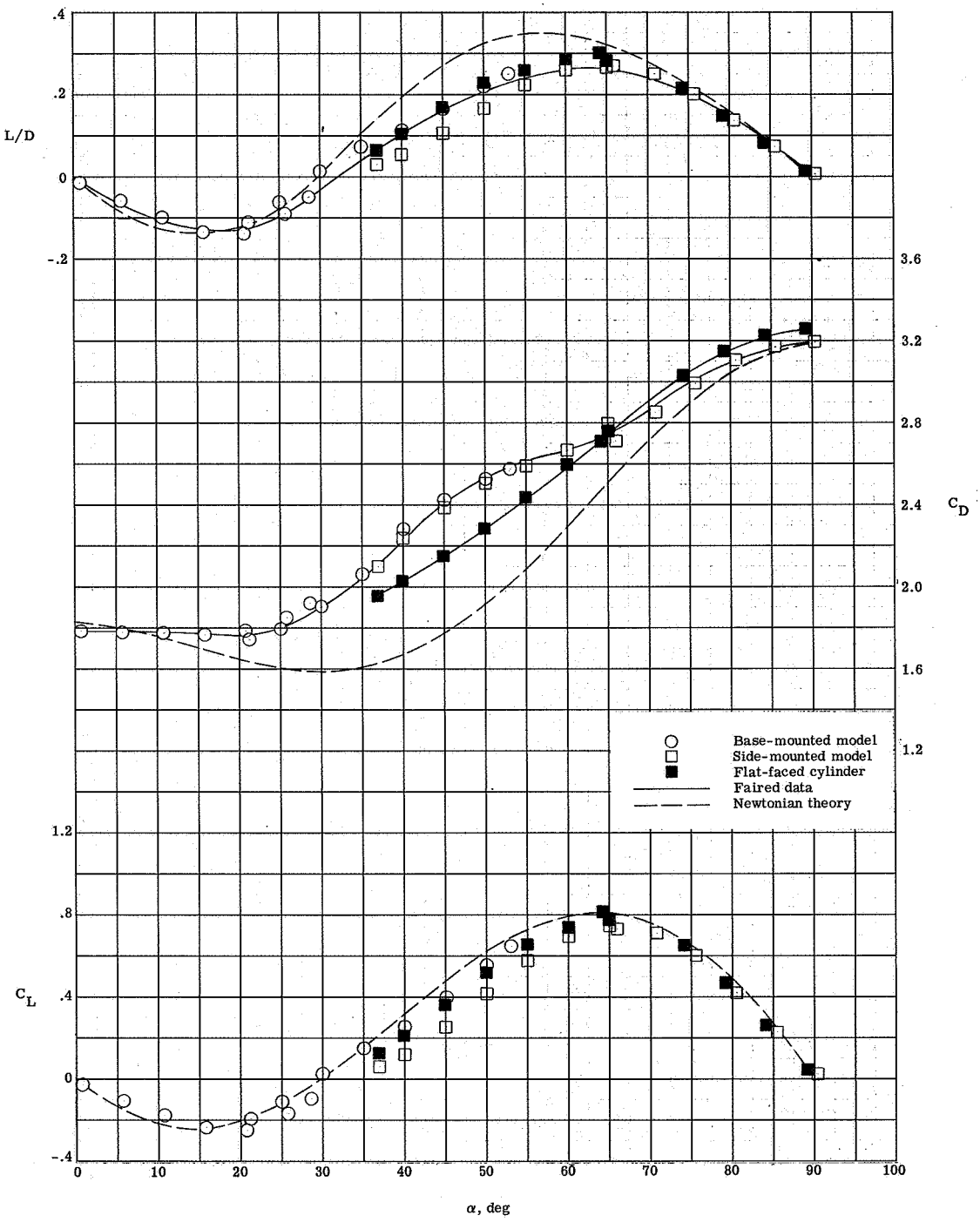

(b) Stability axis.

Figure 7.- Concluded.

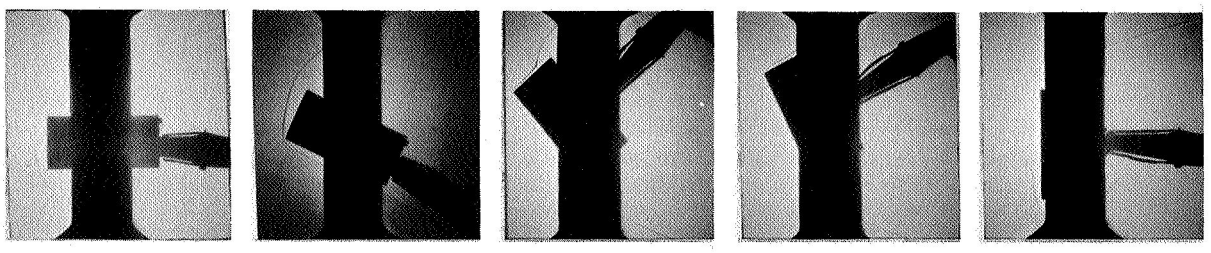

$\alpha = 1.0^{o}$ $\alpha = 25.0^{o}$ $\alpha = 50.1^{o}$ $\alpha = 65.1^{o}$ $\alpha = 95.5^{o}$

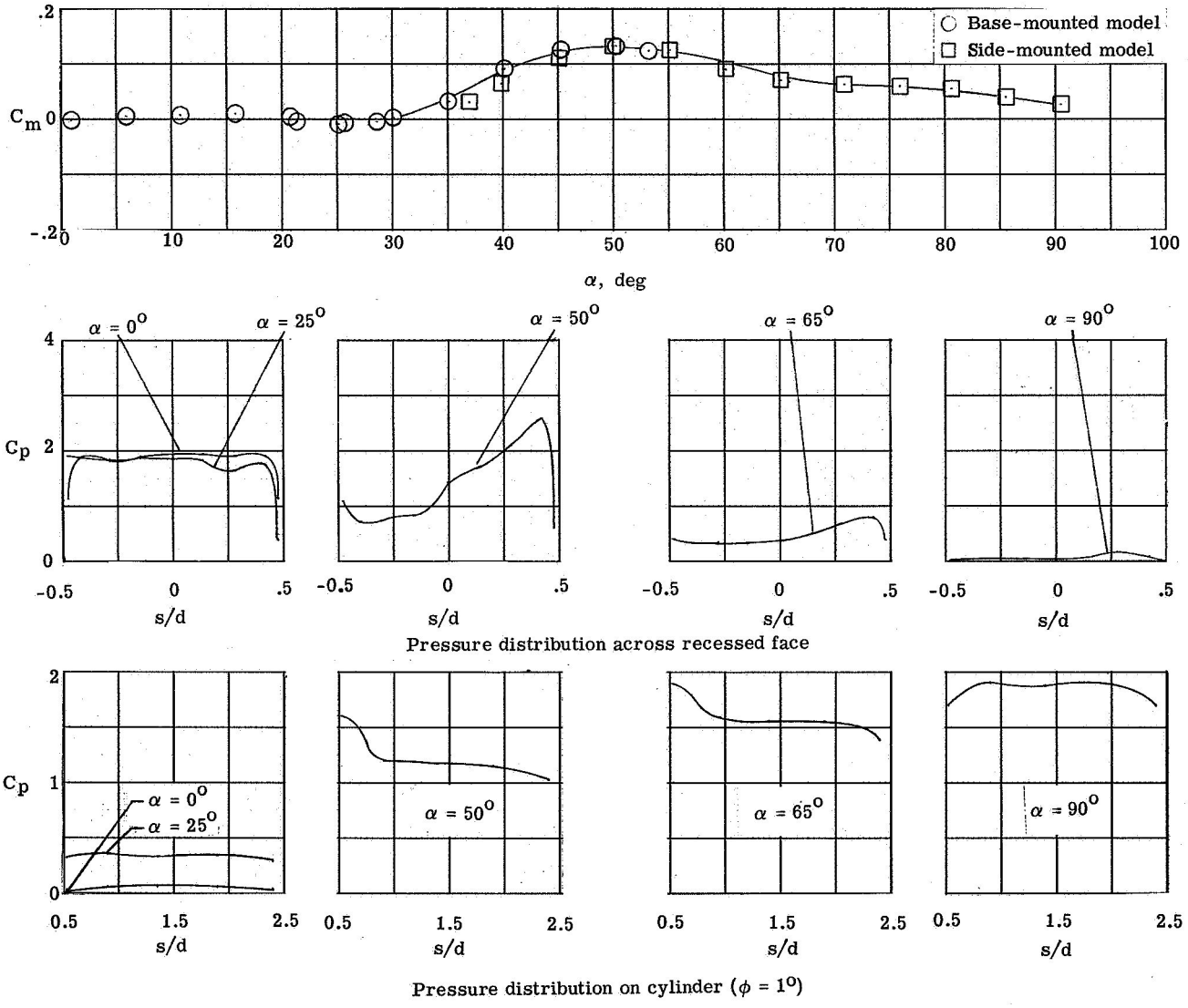

Figure 8.- Comparison of pressure distribution with pitching moment. L-67-6665